



Suppression of Complex Fingerlike Patterns at the Interface between Air and a Viscous Fluid by Elastic Membranes

D. Pihler-Puzović,¹ P. Illien,^{1,2} M. Heil,¹ and A. Juel¹

¹*Manchester Centre for Nonlinear Dynamics and School of Mathematics, University of Manchester, Oxford Road, Manchester M13 9PL, United Kingdom*

²*Département de Physique, École Normale Supérieure, 24 rue Lhomond, 75005 Paris, France*

(Received 24 August 2011; published 14 February 2012)

Growth of complex dendritic fingers at the interface of air and a viscous fluid in the narrow gap between two parallel plates is an archetypical problem of pattern formation. We find a surprisingly effective means of suppressing this instability by replacing one of the plates with an elastic membrane. The resulting fluid-structure interaction fundamentally alters the interfacial patterns that develop and considerably delays the onset of fingering. We analyze the dependence of the instability on the parameters of the system and present scaling arguments to explain the experimentally observed behavior.

DOI: 10.1103/PhysRevLett.108.074502

PACS numbers: 47.15.gp, 47.20.Ma, 47.55.N-

Flow-induced elastic deformations underpin a wide variety of natural processes, from the geophysics of laccolith formation [1] to the physiology of pulmonary airway re-opening [2,3]. In the latter the elastic walls of the airways interact with a free-surface flow, yielding complex and sometimes unexpected behavior [4]. Similar fluid-structure interaction arises in industrial applications, where elastic boundaries are introduced to control processes such as roll coating [5], or change the fluid motion in porous media [6]. In this Letter, we study liquid displacement by air injection into a Hele-Shaw cell and report the suppression of the well-known viscous fingering instability, when the upper boundary of the cell is replaced by an elastic membrane (Fig. 1).

Viscous fingering in rigid-walled Hele-Shaw cells is an archetype for front-propagating, pattern forming phenomena [7–9]. It arises when the fluid is injected at a sufficiently fast rate so that viscous forces exceed surface tension forces, causing the axisymmetric interface between the two fluids to become linearly unstable to nonaxisymmetric perturbations. The nonlinear growth of this instability causes the development of distinct fingers whose tips subsequently become unstable themselves, leading to so-called tip splitting. Repeated tip splitting combined with the arrest of the interface after the passage of the finger tips ultimately creates a complex dendritic pattern as shown in Fig. 1(c). However, if one of the bounding plates is replaced by a latex membrane, we find that the instability is suppressed and the interface remains axisymmetric [Fig. 1(a)] for values of the injection rate at which the rigid system already exhibits strongly nonlinear interfacial growth [Fig. 1(c)]. The critical injection rate beyond which the axisymmetrically expanding interface becomes unstable [Fig. 1(b)] is considerably higher than the corresponding value for the rigid system. Wall elasticity not only affects the onset of the instability but also has a strong impact on the structure of the fingers that develop

subsequently as illustrated in Fig. 1(b). In the elastic cell the entire interface propagates so that a large number of very short fingers develop, which are reminiscent of the printer's instability [10], and contrast with the characteristic dendritic pattern shown in Fig. 1(c). Hence, elastic boundaries offer a novel way to control and suppress nonlinear pattern formation in Hele-Shaw cells, which is considerably more effective than the use of non-Newtonian fluids [11,12], geometric perturbations [13], and the nonlinear control of the injection rate, either by itself [14,15] or in combination with the controlled separation of the (rigid) bounding plates [16].

We performed a series of experiments in the elastic-walled Hele-Shaw cell shown schematically in Fig. 1(d). The bottom boundary was a 15 mm thick float-glass plate, accurately levelled to within 0.1° , and the top boundary was a latex sheet (Supatex) of uniform thickness in the range $0.33 \pm 0.01 \leq h \leq 0.97 \pm 0.01$ mm [17], with a measured Young's modulus of $E = 1.44 \pm 0.05$ MPa. A second latex sheet with a circular cutout of diameter 350 mm was used to separate the two boundaries, and set the initial depth of the cell to values in the range $0.46 \pm 0.01 \leq b_0 \leq 0.79 \pm 0.02$ mm [18].

Prior to each experiment, the cell was filled with silicone oil (Basildon Chemicals Ltd, $\mu = 1.04$ kg m⁻¹ s⁻¹ at 20.3 °C), which wets both glass and latex. The injected oil displaced the less viscous air that initially filled the cell, thus producing a stable, radially expanding oil layer. Placing a second glass plate on top of the bounding elastic membrane during the filling procedure ensured that the elastic membrane remained undeformed until the start of each experiment, and that the initial thickness of the fluid layer was set uniformly to b_0 . A small circular air bubble of approximately 10 mm diameter was injected through the inlet at the start of every experiment to impose controlled initial conditions. The flow source was a compressed nitrogen cylinder, whose flow rate was set manually by a fine needle valve

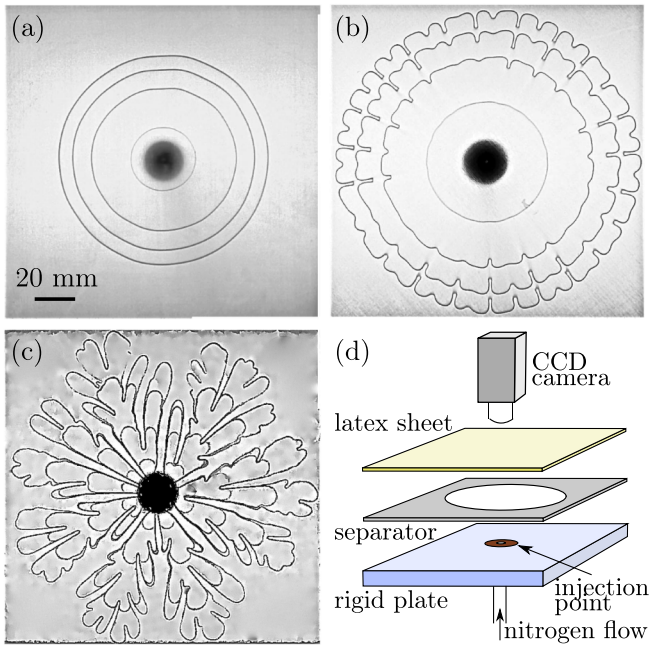


FIG. 1 (color online). (a)–(c) Top view of the front propagation in a radial Hele-Shaw cell in which a growing air bubble displaces viscous fluid that occupies the narrow gap between two parallel plates. Fluids are injected through a small nozzle with an internal diameter of 2.28 mm embedded in a brass fitting, which is mounted flush with the lower bounding plate of the cell and appears as the central black circle. Four successive positions of the interface are shown in each image, with the smallest interface recorded $t = 0.4$ s after air injection started: (a) elastic cell with membrane a; see [17], separator b; see [18], $Q = 145 \text{ cm}^3 \text{ min}^{-1}$, $\Delta t = 4.28$ s; (b) same elastic cell as in (a) with $Q = 1250 \text{ cm}^3 \text{ min}^{-1}$, $\Delta t = 0.71$ s; (c) rigid cell, $Q = 145 \text{ cm}^3 \text{ min}^{-1}$, $\Delta t = 0.57$ s. (d) Schematic diagram of the experimental apparatus.

in the range $50 \leq Q \leq 1300 \text{ cm}^3 \text{ min}^{-1}$, and monitored accurately using a mass airflow meter (Red-Y Smart Meter PCU1000, Icenta Controls Ltd) to remain constant to within $\pm 0.5\%$ of its set value. The flow rate set prior to each experiment could be replicated to within 3%. With these flow parameters, the load on the upper boundary was insufficient to cause buckling instabilities of the latex membrane. A three-way pneumatic solenoid valve was used to switch the gas flow from exiting into the atmosphere to entering the cell at the start of each experiment. We either monitored the time evolution of the backlit free surface by recording top view movies of the pattern formation with a CCD camera (1360×1024 pixels) at a rate of 7.5 frames per second, or measured the sheet inflation by projecting a line onto the elastic upper boundary with a video projector positioned vertically above the cell, and recording its deformation with a still camera (Nikon D2X/s) oriented at 60° with respect to the light sheet.

In the elastic cell, the interface displaces the viscous liquid at a lower speed than in the rigid configuration because the imposed load causes the sheet to inflate,

resulting in a nontrivial fluid-structure interaction problem. We measured the time evolution of the average radius of the expanding bubble and found that it scaled with time as $\langle r \rangle \sim t^{0.37}$ for all values of the experimental parameters [see Fig. 2(a)]. To explain this behavior we follow the approach taken in [3] and predict the evolution of $\langle r \rangle$ by defining two distinct regions on either side of the bubble interface [see Fig. 2(b)], and matching the slopes of the deformed sheet obtained in regions I and II at the interface. At any time t , the volume of the injected air is Qt . The deformation measurements of the membrane showed its shape to be approximately self-similar and $\langle r \rangle \gg H \gg b_0$, so that $Qt \sim \langle r \rangle^2 H$, where H is the vertical displacement of the elastic sheet at its center. Therefore, the membrane slope in region II varies like $\theta_{II} \sim Qt / \langle r \rangle^3$. The vertical displacement of the elastic sheets used in this study is largest in region II, reaching up to 5.5% of the bubble diameter at the point of maximum deflection [see Fig. 2(b)]. For vertical displacements $> 1\%$ in an empty elastic cell with wall thicknesses [17], both membrane inflation experiments and numerical simulations using the multiphysics finite-element library OOMPH-LIB [19] indicate that the membrane response is nonlinear and strongly affected by self-induced tension. However, the deformation of the membrane ahead of the interface (region I) is considerably smaller, because the membrane is constrained by lubrication forces in the viscous layer. Hence, we can assume a linear elastic response of the membrane in region I, so that its small transverse (out-of-plane) displacement b , subject to the distributed load p ,

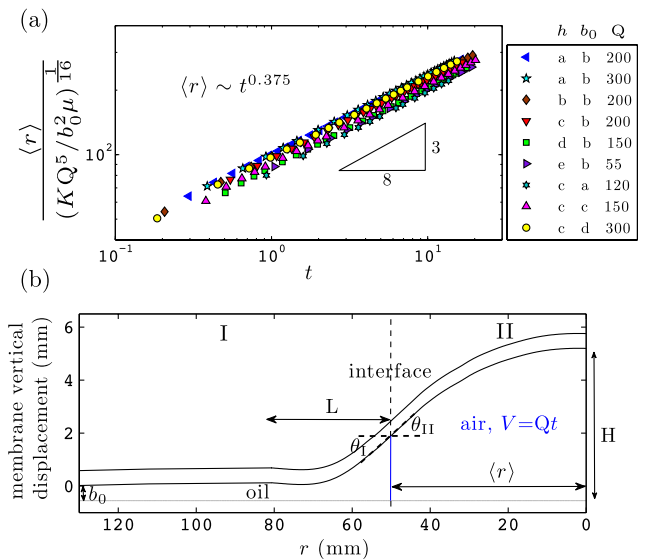


FIG. 2 (color online). (a) Dependence of scaled $\langle r \rangle$ (in units of $\text{mm s}^{-3/8}$) on t (in s), both on a logarithmic scale, for different experimental runs (h and b_0 are given in [17,18], respectively; units of Q are $\text{cm}^3 \text{ min}^{-1}$). (b) Displacement of membrane c for separator b and $Q = 50 \text{ cm}^3 \text{ min}^{-1}$ at $t = 69$ s from the start of the experiment.

is given by $p = K\nabla^4 b$, where $K = Eh^3/12(1 - \gamma^2)$ is the bending stiffness of the membrane and $\gamma \approx 0.5$ is Poisson's ratio. Furthermore, we assume that the relation between the depth-averaged fluid velocity v and the pressure is given by the lubrication equation $v = -\frac{b^2}{12\mu}\nabla p$. Balancing bending and lubrication pressures in this region gives the velocity scale $U \sim Kb_0^3/\mu L^5$. By estimating U as $\langle r \rangle/t$, we predict the scaling for the slope of the sheet in this region as $\theta_1 \sim b_0/(Kb_0^3 t/\mu \langle r \rangle)^{1/5}$. Matching the slopes at the interface, $\theta_1 \sim \theta_{II}$, gives

$$\langle r \rangle \sim (KQ^5/b_0^2\mu)^{1/16}t^{3/8} \sim t^{0.375}. \quad (1)$$

Given the simplicity of our model, the predicted scaling exponent is in remarkable agreement with the experimental measurements shown in Fig. 2(a); the slight spread of the data in this figure is likely to be due to the many secondary effects that we ignored in our analysis, such as nonlinearities in the behavior of the sheet.

In order to determine the onset of instability, we processed experimental images using Matlab edge detection routines to extract the length of the interface, $\tilde{\ell}$, and the length of its convex envelope, ℓ , as shown in Fig. 3(a). In the absence of an instability, $\delta_\ell = \tilde{\ell} - \ell = 0$ [Fig. 3(b)]. As the bubble expands, the unstable interface deforms into fingers that grow, saturate, and each split into two second-generation fingers; a process that repeats itself leading to a continual increase in the number of fingers. The excess perimeter, $\delta_\ell > 0$, is a measure of instability, which combines information about the depth and number of fingers. An example of the variation of δ_ℓ with the mean radius $\langle r \rangle$ is shown in Fig. 3(b). Following the onset of instability, δ_ℓ

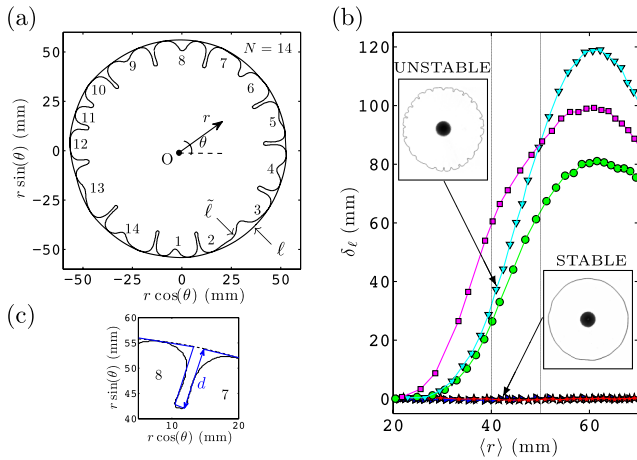


FIG. 3 (color online). (a) Typical image analysis procedure—the corresponding experimental run is presented in Fig. 4(j). (b) The excess perimeter $\delta_\ell = \tilde{\ell} - \ell$ as a function of the average interfacial radius $\langle r \rangle$ for membrane a, see [17], separator b, see [18], and several experimental runs with injection rates $Q = 200 \text{ cm}^3 \text{ min}^{-1}$ (“stable”) and $Q = 700 \text{ cm}^3 \text{ min}^{-1}$ (“unstable”). (c) Close-up of fingers 7 and 8 from (a) with the schematics for defining the depth d .

initially increases up to a maximum value, and then decays as the bubble expands further. This is because the flow rate Q is held constant, so that the interface decelerates as it expands. Hence, the interface always restabilizes for sufficiently large values of $\langle r \rangle$, for which the interface speed falls below its critical threshold for instability. Even though the maximum value of δ_ℓ varies significantly between experiments, δ_ℓ reaches its maximum value at the same $\langle r \rangle$; see Fig. 3(b). The variations between experiments are a direct result of the system's sensitivity to the initial configuration, which was inevitably slightly nonaxisymmetric. Hence, the interface did not display a perfect spatially periodic pattern during the initial stages of the instability, and the unstable interface therefore always comprised fingers at different stages of their evolution. The observed variability in δ_ℓ in Fig. 3(b) results from different distributions of developing and splitting fingers at given $\langle r \rangle$ in successive experimental runs. Because of this variability, five experimental runs were performed for each set of parameters. The averaged depth of the fingers, $\langle d \rangle$, was determined by counting the number N of fingers in the pattern [20] as illustrated in Fig. 3(a). Assuming that the depth of the finger provides the main contribution to the excess perimeter as shown in Fig. 3(c), we define $\langle d \rangle = \delta_\ell/(2N)$. We then characterized the growth of the instability by comparing $\langle d \rangle$ at average radii $\langle r \rangle = 4 \text{ cm}$ and $\langle r \rangle = 5 \text{ cm}$, which covered the region in which the instability tended to grow most rapidly [see Fig. 3(b)], and define the parameter $\Delta = \langle d \rangle(\langle r \rangle = 5 \text{ cm}) - \langle d \rangle(\langle r \rangle = 4 \text{ cm})$.

The variation of Δ with Q for each elastic sheet is shown in Fig. 5. For low values of Q , we have $\Delta = 0$, indicating stable interfaces such as the one shown in Fig. 4(a). Once Q exceeds a certain threshold Q_c , Δ grows approximately linearly with Q [Fig. 4(b) and 4(c)], until the instability saturates [Figs. 4(d) and 4(e)]. We fit the growth region using linear least squares and determine the critical flow rates Q_c by extrapolating this fit for each data set, as shown in Fig. 5. The rate at which the fingers grow increases with

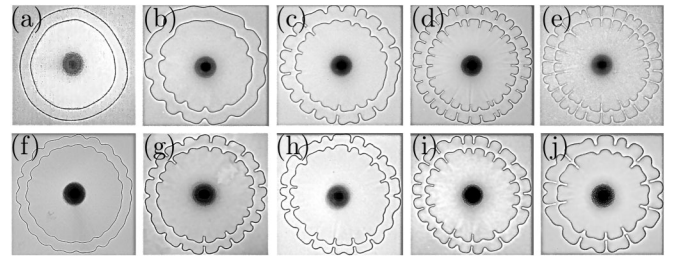


FIG. 4. Superimposed snapshots of the interface when $\langle r \rangle = 4 \text{ cm}$ and $\langle r \rangle = 5 \text{ cm}$. First row: the variation in the typical top view for membrane $h = 0.69 \pm 0.02 \text{ mm}$, $b_0 = 0.56 \pm 0.02 \text{ mm}$, and injection flow rates $75 \text{ cm}^3 \text{ min}^{-1}$ (a), $200 \text{ cm}^3 \text{ min}^{-1}$ (b), $500 \text{ cm}^3 \text{ min}^{-1}$ (c), $700 \text{ cm}^3 \text{ min}^{-1}$ (d), and $900 \text{ cm}^3 \text{ min}^{-1}$ (e); second row: the variation in the typical top view for $Q = 400 \text{ cm}^3 \text{ min}^{-1}$, $b_0 = 0.56 \pm 0.02 \text{ mm}$, for sheet thicknesses given in [17] increasing from left to right.

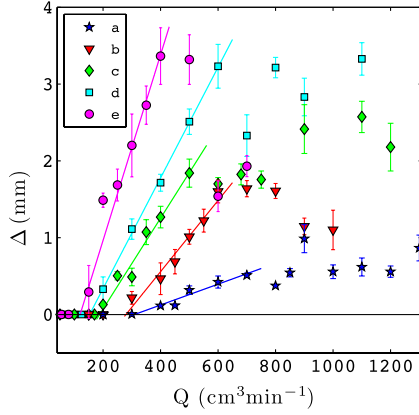


FIG. 5 (color online). Dependence of Δ on injection flow rates Q for the different membranes given in [17].

the membrane thickness, with the fingers being deeper and saturating faster for larger h [see Figs. 5 and 4(f)–4(j)]. This limited the range of membrane thicknesses for which the onset could be reliably determined with the chosen method to that shown in Fig. 5. Another series of experiments was performed to investigate the effect of variations of the initial fluid depth b_0 on Q_c . Results are presented in Fig. 6 which shows that $Q_c \sim K^{-0.30 \pm 0.05}$ [Fig. 6(a)] and $Q_c \sim b_0^{1.72 \pm 0.14}$ [Fig. 6(b)]. These scalings were determined from least-square power-law fits to the experimental data.

To explain these scalings we recall that destabilizing viscous forces and restoring bending forces are the dominant effects in the system's behavior, and now examine the length scales on which they act. Suppression of the fluid-mechanical instability by the deformation of the membrane requires the length scale L_b of the bending deformation to be smaller than the viscous length scale L_v . Lubrication theory gives $L_v \sim Pb_0^2/U\mu$. Using the equation for the small transverse displacement of the membrane we estimate that the bending forces act on a length scale $L_b \sim (Kb_0/P)^{1/4}$. By balancing these two length scales ($L_b \sim L_v \sim L$), and considering that at fixed radius from the injection point the velocity of the propagating interface is proportional to Q , we obtain the scaling

$$Q_c \sim K^{-1/4} b_0^{7/4} P^{5/4} \mu^{-1} \quad (2)$$

for the onset of instability. The exponents on K and b_0 are in excellent agreement with our experimental findings in Fig. 6 which implies the surprising result that at the onset of instability P is approximately independent of K and b_0 .

To summarize, we have shown that elastic boundaries are surprisingly effective in suppressing viscous fingering in a Hele-Shaw cell. The onset of instability is delayed significantly because the membrane deformations reduce destabilizing pressure perturbations ahead of the propagating interface. Experimental findings are strongly supported

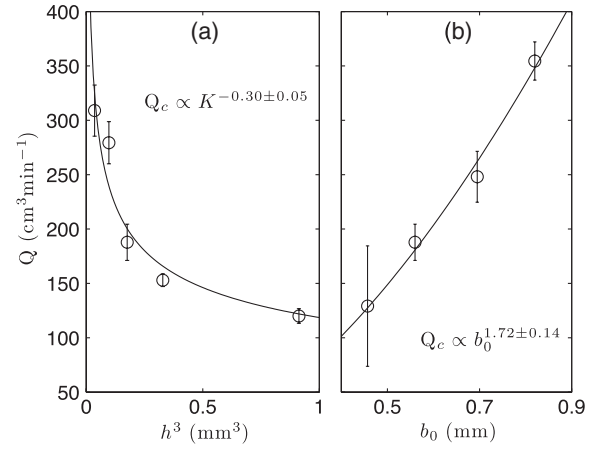


FIG. 6. The critical injection flow rate at the onset of the instability for (a) different latex sheets and (b) different separators at $\langle r \rangle = 5$ cm.

with the scaling arguments based on a bending model for the deformation of the elastic sheet and lubrication theory for the fluid flow. Similar mechanisms operate in a wide range of fluid-structure interaction problems [1–6]. Therefore, development of more detailed quantitative predictions for our system could directly benefit a number of practical applications. This will require the careful consideration of both nonlinear deformations of the sheet in the bubble region (region I) and matching boundary conditions at the interface. Such work is on its way.

The authors thank A.L. Hazel, T. Mullin, and O.E. Jensen for useful discussions. D.P.P. would like to thank DAMTP, University of Cambridge and School of Mathematics, University of Manchester for funding her through the Crighton Fellowship and MAPLE grant, respectively. A.J. thanks EPSRC for their support through an Advanced Research Fellowship.

-
- [1] C. Michaut, *J. Geophys. Res.* **116**, B05205 (2011).
 - [2] M. Heil and A. Hazel, *Annu. Rev. Fluid Mech.* **43**, 141 (2011).
 - [3] O.E. Jensen, M. Horsburgh, D. Halpern, and D.P.G. III, *Phys. Fluids* **14**, 443 (2002).
 - [4] A. Heap and A. Juel, *Phys. Fluids* **20**, 081702 (2008).
 - [5] M.S. Carvalho and L. Scriven, *J. Fluid Mech.* **339**, 143 (1997).
 - [6] W. Ehlers and J. Bluhm, *Porous Media: Theory, Experiments, and Numerical Applications* (Springer, New York, 2002).
 - [7] P. Saffman and G. Taylor, *Proc. R. Soc. A* **245**, 312 (1958).
 - [8] L. Paterson, *J. Fluid Mech.* **113**, 513 (1981).
 - [9] J.D. Chen, *J. Fluid Mech.* **201**, 223 (1989).
 - [10] A.D. McEwan and G.I. Taylor, *J. Fluid Mech.* **26**, 1 (1966).
 - [11] A. Lindner, D. Bonn, and J. Meunier, *J. Phys. Condens. Matter* **12**, A477 (2000).

- [12] P. Fast, L. Kondic, M. J. Shelley, and P. Palffy-Muhoray, *Phys. Fluids* **13**, 1191 (2001).
- [13] M. Rabaud, Y. Couder, and N. Gérard, *Phys. Rev. A* **37**, 935 (1988).
- [14] S. Li, J. S. Lowengrub, J. Fontana, and P. Palffy-Muhoray, *Phys. Rev. Lett.* **102**, 174501 (2009).
- [15] C.-Y. Chen, C. W. Huang, L. C. Wang, and J. A. Miranda, *Phys. Rev. E* **82**, 056308 (2010).
- [16] E. O. Dias and J. A. Miranda, *Phys. Rev. E* **81**, 016312 (2010).
- [17] Membrane thicknesses: (a) $h = 0.33 \pm 0.01$ mm; (b) $h = 0.46 \pm 0.01$ mm; (c) $h = 0.56 \pm 0.02$ mm; (d) $h = 0.69 \pm 0.02$ mm; (e) $h = 0.97 \pm 0.01$ mm.
- [18] Separator thicknesses: (a) $b_0 = 0.46 \pm 0.01$ mm; (b) $b_0 = 0.56 \pm 0.02$ mm; (c) $b_0 = 0.69 \pm 0.02$ mm; (d) $b_0 = 0.79 \pm 0.02$ mm.
- [19] <http://www.oomph-lib.org>
- [20] A criterion was chosen for splitting fingers, whereby a finger was counted as a single unit if the emerging tips were less than one half of the original finger depth.